Beneficial *vs.* Inhibiting Passivation by the Native Lithium Solid Electrolyte Interphase Revealed by Electrochemical Li^+ Exchange

Gustavo M. Hobold[1], Kyeong-Ho Kim[1], Betar M. Gallant[1,*]

[1]Department of Mechanical Engineering, Massachusetts Institute of Technology, Cambridge, MA 02139
*bgallant@mit.edu

Abstract

Despite being a leading candidate to meet stringent energy targets of Li-ion batteries, the lithium (Li) metal anode has yet to achieve Coulombic efficiency (CE) requirements for long cycle life (>99.9%), particularly at high rates (>1 C). These limitations derive from the native solid electrolyte interphase (SEI) which, among multiple functions, stabilizes and protects deposited Li. The SEI also plays a critical role in regulating Li^+ exchange between the electrolyte and the electrode, but quantification of this effect has been non-straightforward, and a general relationship between Li^+ exchange and CE has not been clearly elucidated to date. Using electrochemical impedance and voltammetry, we report self-consistent Li^+ exchange values of native SEIs over a range of relevant electrolytes with CE spanning 78.0% to >99%. CE and its retention at high rates are found to be positively correlated with the rate of SEI Li^+ exchange. Additionally, Li^+ exchange rates increased during cycling in high-CE electrolytes, in some cases by an order of magnitude to exceed 10 mA/cm^2, whereas for low-CE electrolytes they remained low (<1 mA/cm^2), revealing a chemistry-dependent picture of SEI evolution with often-complex dynamics. The evolution in Li^+ exchange unique to high-CE electrolytes also provides insights into the role and effectiveness of the formation cycle on Cu current collectors upon the first plating step. Altogether, these findings indicate that Li^+ exchange governs several key processes related to Li deposition and cycling efficiency. Consequently, its quantification can help to guide future high-CE electrolyte design, particularly targeting high rates (> 1 mA/cm^2).

Introduction

The lithium (Li) metal anode is the most compelling alternative to today's graphite anodes for meeting stringent gravimetric energy targets (>500 Wh/kg) in Li-ion batteries, as it allows a theoretical 10-fold upgrade in capacity (3860 mAh/g *vs*. 372 mAh/g) at comparable electrode potential. Unlike graphite, Li reversibility in liquid electrolytes, as quantified by Coulombic efficiency (CE) – the ratio between the stripping and plating capacity onto a non-Li substrate such as Cu – still falls below the >99.9% required for >1000 cycles, although electrolytes exceeding 99% CE for at least a portion of cycle life are increasingly common.[1, 2] The Li anode also displays rate capability well below the requirements for fast charge (>2 C).[3] These gaps have motivated extensive efforts in increasing CE through electrolyte and interface design.[4] Cycling inefficiencies associated with the Li anode reflect a loss of cyclable Li^0 inventory from the cell. Hence, these inefficiencies can manifest in two ways: electrolyte reduction with concerted consumption of Li^0 to form the solid electrolyte interphase (SEI), and as disconnected metallic Li^0 that becomes electronically stranded during cycling.[5-7] Typically, capacity loss due to SEI formation, rather than to metallic Li^0, predominates at higher CE where deposition is more uniform and less porous.[5, 8] Once formed, an imperfect SEI may invite further non-uniform Li/plating stripping[2] and SEI breakage, which necessitates its sustained formation on subsequent cycles.

Critically, the SEI also regulates transport of Li^+ ions between electrolyte and electrode. As such, the presence of an SEI can have profound effects on transport and kinetics at the interface. For instance, cyclic voltammetry of Li plating/stripping on microelectrodes at ultrafast scan rates (*e.g.*, > 10 V/s, **Fig. 1**, left), which are fast enough to disrupt the native SEI, have found that the intrinsic kinetics of Li plating/stripping, as parametrized by a formal exchange current j_0,[9] can be as high as ~40 mA/cm^2 in carbonate-based electrolytes.[10] However, chemical Li^+ exchange rates, as determined by nuclear magnetic resonance (NMR) measurements on a pristine SEI soaked in similar carbonate electrolytes, have been reported to be substantially lower at ~0.5-3 mA/cm^2.[11] These lower values correspond to charge-transfer resistances up to ~100-fold[10] higher compared to an SEI-less interface imposed by the ultrafast scan rates, indicating that the SEI can substantially bottleneck Li^+ exchange.

Earlier attempts to quantify j_0 under more-realistic operating conditions with an SEI present focused largely on carbonate-based electrolytes (**Table S1**). In those studies, numerical values of

j_0 were variable, *e.g.* reported values of j_0 varied by over one order of magnitude for 1 M $LiClO_4$ in propylene carbonate (PC) across different studies,[12, 13] which may relate in part to how the Li electrode was prepared and/or aged, as well as which experimental technique was used. Despite some scatter in the data, however, meaningful differences across electrolytes can begin to be discerned. For instance, j_0 was reported to range between 0.1–0.3 mA/cm^2 (0.1 M)[14, 15] or 0.95–1.8 mA/cm^2 (1 M)[14, 15] for $LiClO_4$ in PC, indicating that j_0 can be sensitive to salt concentration. Similarly, j_0 was found to have a lower range in 1 M $LiPF_6$ PC (0.3–2.2 mA/cm^2)[16, 17] than 1 M $LiBF_4$ PC (0.5–7.5 mA/cm^2)[16, 17], suggesting that the anion also influences j_0. Exchange current values have also been reported to a more limited extent in ethers. In those solvents, j_0 again exhibited sensitivity to the salt anion, ranging between 1.4–3.6 mA/cm^2 for 1 M $LiPF_6$, $LiClO_4$, $LiBF_4$ and $LiAsF_6$ in 2-methyl-tetrahydrofuran, 2-Me-THF, in increasing order.[17] Similarly, the relative volume fraction of ether blends can affect j_0, reported to range between 2.5–7 mA/cm^2 for 1 M $LiAsF_6$ in blends of diethyl ether, DEE, and tetrahydrofuran, THF.[18]

Whether any clear and universal relationship between j_0 and CE exists has remained less clear, however. This is largely because comprehensive data for j_0, as well as concurrently measured CE, are missing across a wide range of electrolytes. Moreover, prior reports have presented conflicting interpretations of whether higher j_0 is beneficial[19-22] (hence desired) or detrimental[17, 23-25] (hence to be avoided) for promoting Li reversibility, sometimes based on relatively limited data sets. For example, experiments in tetraethylene glycol dimethyl ether (TEGDME)-based electrolytes led to a conclusion that higher j_0 leads to lower CE.[24] In contrast, other studies have reported that incorporation of additives such as FEC[19] or $SiCl_4$[21] into a carbonate electrolyte increases both j_0 and CE. As noted, one challenge in generalizing these observations arises, in part, from variable measurement and analysis protocols, *e.g.*, microelectrode[17, 23, 25] *vs.* coin cells[19-22], and/or slow (< 100 mV/s)[17, 19, 21, 22] *vs.* fast (> 100 mV/s)[23, 25] scan rates (**Table S1**) used by different groups.

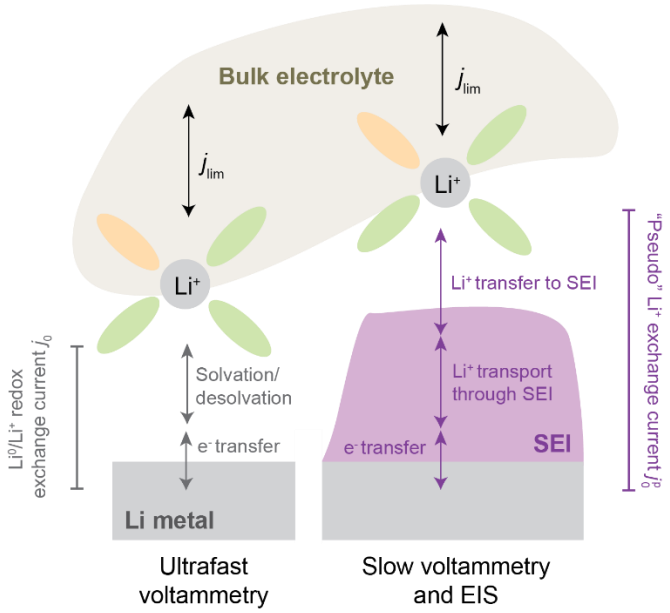

Fig. 1 Illustration of processes involved in Li^0/Li^+ redox from bulk electrolyte to the Li metal electrode, without (left) and with (right) an SEI present. At left, j_0 refers to a classically defined[9] exchange current density [mA/cm^2] that reflects the intrinsic kinetics of electron transfer coupled to (de)solvation and ion transfer of Li^+ to form Li^0. It is probed experimentally by ultrafast voltammetry, typically using microelectrodes. With an SEI present, electron transfer, (de)solvation and Li^+ transfer become impeded by an SEI, which itself has electrolyte-dependent properties. Experiments under such conditions report on an apparent or "pseudo"-exchange current density regulated by an SEI, herein denoted j_0^p. The above schematic assumes negligible electronic conductivity throughout the SEI and makes no assumptions about its microstructure or charge-transport mechanisms, other than being dominated by Li^+ as charge carrier.

In this context, there is a significant need for quantification of Li^+ exchange under practical battery conditions and elucidation of its dependence on electrolyte chemistry, testing protocol, and rate. In this study, Li^+ exchange at the Li anode is systematically quantified using cyclic voltammetry (CV) at slow scan rates (1 mV/s) and electrochemical impedance spectroscopy (EIS), both of which intentionally allow an SEI to develop natively (**Fig. 1**, right). In order to span a diverse set of SEI chemistries of interest, we employ a selection of historically-relevant and more modern, high-performance electrolytes. Given that Li^+ exchange is both electrode-history- and surface-area- dependent, we interpret the exchange rates in the framework of a "pseudo"-exchange

current, j_0^p, that represents the total rate of Li^+ exchange on the electrode. j_0^p is found to vary considerably across electrolytes, with an unambiguous positive correlation with CE consistent across different measurement protocols. In addition, tracking of j_0^p evolution upon cycling reveals unexpected dynamic behaviors that allow for new insights into the evolution of electrochemically-active surface area and SEI quality upon cycling. These findings provide a new approach for future efforts to develop high-rate and high-CE electrolytes by considering how to maximize the SEI rates of Li^+ exchange.

Measuring Li^+ exchange through impedance spectroscopy

Representative electrolytes were selected for analysis to span a range of reported CE values based on a previous comprehensive literature analysis.[4] The electrolytes (**Fig. 2a**) included 1.5 M $LiAsF_6$ in 2-Me-THF (CE = 78.0%); conventional and fluorinated carbonates of 1 M $LiClO_4$ in PC (81.9%), 1 M $LiPF_6$ in EC/DEC (93.8%), 1 M LiFSI in FEC (95.3%) or 1 M $LiPF_6$ in EC/DMC (96.9%); and higher-concentration fluorinated carbonates of 2 M and 7 M LiFSI in FEC (97.5% and 98.2%, respectively). Finally, two additive-containing electrolytes were examined: 1 M LiTFSI in DOL/DME and 2 M LiFSI/1 M LiTFSI in DOL/DME, each containing 3wt% $LiNO_3$ (99.0% and 99.3%, respectively). All CE values were measured using a pre-formation/reservoir cycling protocol following Adams *et al.*[26] as described further in the Experimental methods (**Fig. S1**, ESI). These values generally agree well with prior literature reports (**Table S2** and **Fig. S2**, ESI), with small variations likely explained by the difference in CE protocols between the original reports and the methodology used herein.

Before examining the proposition that SEI can be a relevant factor that limits, and thus determines, electrochemical measures of Li^+ exchange, we first examined possible relationships between CE and two key bulk electrolyte properties. First, Li^+ diffusivity in the bulk electrolyte (*D*), which governs mass transport upon Li^+ plating,[2, 9, 27] was measured using diffusion-ordered spectroscopy (DOSY) NMR. Values of *D* ranged from 8.90×10^{-8} cm^2/s for 7 M LiFSI FEC to 3.42×10^{-6} cm^2/s for 1 M LiTFSI DOL/DME + 3wt% $LiNO_3$ (**Fig. S3**, ESI). No clear relationship with CE was observed. Additionally, we also examined the ^7Li chemical shift in liquid NMR, which has been shown to reflect the degree of contact-ion pairing when compared between electrolytes of alike solvent (*e.g.*, varying anion chemistry and/or concentration in the same

solvent).[28] Under these circumstances, ^{7}Li chemical shift has been shown to correlate with CE[29] and intrinsic j_0 (*i.e.*, absent an SEI).[10] Here, however, when compared over electrolytes of dissimilar chemistry (*e.g.*, different salt and solvent chemistries), ^{7}Li chemical shift did not reveal a correlation with CE (**Fig. S3**, ESI). These observations indicate that intrinsic properties measured at the bulk electrolyte level are not directly predictive of CE measured under conditions that permit an SEI to form.

Now considering the presence of the SEI, Li^+ exchange currents were first measured using EIS analysis in symmetric Li/Li cells. **Fig. 2b** shows a typical protocol. Following cell assembly, an initial impedance spectrum, denoted by an open blue circle, was conducted in the pristine state ("Pre-cycle EIS") after a 5 h rest at OCV, sufficient to establish a native, intact SEI. This interphase includes artifacts from the preparation and handling of the electrodes.[30] Next, a complete plating/stripping cycle was conducted (0.5 mA/cm^2, 1 mAh/cm^2). Following a 5 min. rest at OCV, which is sufficient to re-form a native SEI[31] but short enough to avoid exacerbated aging effects,[30, 32] a second impedance spectrum was collected. This process repeated subsequently for additional plating/stripping+EIS cycles. **Fig. 2c** shows EIS data over five such cycles for three representative electrolytes (1.5 M $LiAsF_6$ in 2-Me-THF, 1 M $LiPF_6$ in EC/DMC, and 1 M LiTFSI in DOL/DME + 3% $LiNO_3$) corresponding to the colored bars in **Fig. 2a**, with the comprehensive data set for all electrolytes shown in the ESI (**Fig. S4**, ESI). In general, the EIS responses took the form of a single, high-frequency semi-circle with a lower-frequency tail. The semi-circle was fitted by a simple equivalent circuit[33] comprising a parallel RC element associated with charge-transfer and a capacitance-Warburg impedance element associated with Li^+ diffusion across the interphase (see **ESI Note 1** for details).

An exchange current value was extracted from the EIS fitting by $j^{p}_{0,EIS} = kT/(eR_{SEI})$, where k is the Boltzmann constant, T is temperature (297 K), e is the elementary charge and R_{SEI} is the total SEI resistance at 0 Hz (corresponding to constant current) fitted from EIS (Experimental methods and **ESI Note 1**). The parameters R_{SEI} [Ω cm$^2_{\mathrm{geo}}$] and $j^{p}_{0,EIS}$ [mA/cm$^2_{\mathrm{geo}}$, hereafter also denoted simply as mA/cm^2] are normalized to the geometric surface area of the Li electrode, given that the true surface area of plated Li is unknown and may change over the electrode's use. To emphasize this point, we employ the superscript "p" to denote a "pseudo"-exchange current, and to emphasize that $j^{p}_{0,EIS}$ is only intrinsic for a given SEI for a fictitious, planar (uncycled) electrolyte

containing no surface roughness. As we will show, $j^{p}_{0,EIS}$ still has significant physical meaning and provides insights into the properties and behavior of the SEI.

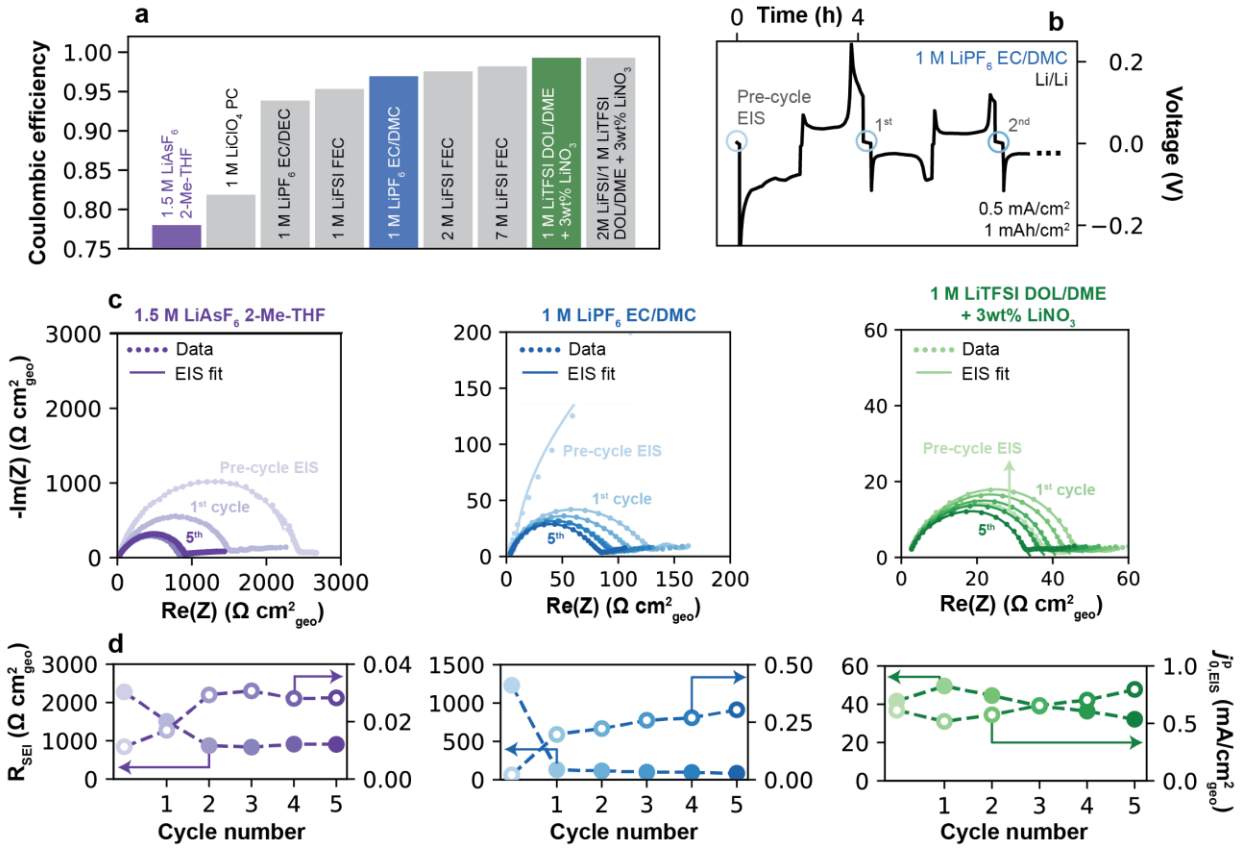

Fig. 2 Measuring Li^+ exchange by electrochemical impedance spectroscopy. (a) CE of electrolytes considered in this study, measured at 0.5 mA/cm² using a pre-formation/reservoir cycling protocol (**Fig. S1**, ESI). (b) Representative galvanostatic plating/stripping cycles in a Li/Li cell in 1 M $LiPF_6$ EC/DMC at 0.5 mA/cm^2 and 1 mAh/cm^2 plating capacity. Blue circles indicate the timesteps at which EIS was collected following a 5 min. rest at OCV. (c) Nyquist plots of Li/Li cells collected pre- and post-cycling in three representative electrolytes: 1.5 M $LiAsF_6$ 2-Me-THF, 1 M $LiPF_6$ EC/DMC, and 1 M LiTFSI DOL/DME + 3wt% $LiNO_3$. Markers indicate raw data, while solid lines represent fits to the high-frequency data points (> 20 Hz) using an equivalent RC-Warburg circuit. (d) SEI resistance and pseudo-exchange current density, $j^{p}_{0,EIS}$, obtained from fitting EIS spectra in (c).

For the studied electrolytes, the pre-cycle EIS spectrum was typically largest in magnitude. Subsequent plating/stripping+EIS iterations consistently yielded smaller semi-circles, attributed to breakage of the original SEI and formation of a thinner native interface. Notably, after 5 cycles the R_{SEI} magnitudes varied significantly across electrolytes (**Fig. 2d**), being highest for 1.5 M $LiAsF_6$ in 2-Me-THF (512.6 Ω cm^2 on cycle 5), followed by 1 M $LiPF_6$ in EC/DMC (47.6 Ω cm^2) and 1 M LiTFSI DOL/DME + 3% $LiNO_3$ (18.3 Ω cm^2). Correspondingly, the $j^p_{0,EIS}$ values across these three electrolytes showed an increasing trend of 0.03, 0.30 and 0.79 mA/cm^2, respectively.

Fig. 3a shows $j^p_{0,EIS}$ measured over 50 cycles for each electrolyte. Over this longer cycling regime, two distinct behaviors in $j^p_{0,EIS}$ evolution were observed, which we denote by "Type 1" and "Type 2". In Type 1 electrolytes, $j^p_{0,EIS}$ remained reasonably stable over 50 cycles, as with 1.5 M $LiAsF_6$ 2-Me-THF, 1 M $LiClO_4$ PC, 1 M $LiPF_6$ EC/DEC, 1 M LiFSI FEC, and 1 M $LiPF_6$ EC/DMC. Owing to the largely unchanging $j^p_{0,EIS}$, a single representative value in each electrolyte can be identified. In Type 2 electrolytes, however, a substantial increase in $j^p_{0,EIS}$ was observed with cycling, as with 2 M LiFSI FEC, 7 M LiFSI FEC, 1 M LiTFSI DOL/DME + 3wt% $LiNO_3$, 2 M LiFSI 1 M LiTFSI DOL/DME + 3wt% $LiNO_3$. In some cases, $j^p_{0,EIS}$ increased by up to two orders of magnitude (**Fig. 3b**), *e.g.*, 1 M LiTFSI DOL/DME + 3wt% $LiNO_3$ increased from 0.25 to ~25 mA/cm^2; however, in no case did $j^p_{0,EIS}$ decrease. Because of these changes, it is not possible to identify a singular representative value of $j^p_{0,EIS}$ in Type 2 electrolytes. Interestingly, Type 1 electrolytes corresponded to those in the lower CE range, namely 1.5 M $LiAsF_6$ (CE = 78.9%) to 1 M $LiPF_6$ EC/DMC (CE = 96.9%), whereas those with higher CE all exhibited Type 2 (increasing $j^p_{0,EIS}$) behavior. We note that $j^p_{0,EIS}$ for 1 M $LiPF_6$ EC/DMC converges to 0.45 ± 0.04 mA/cm^2, which is in excellent agreement with the steady-state values obtained for chemical Li^+ exchange measured recently *via* solid-state NMR (0.47 mA/cm^2) on the native SEI in the same electrolyte.[11] The converged values obtained in other carbonate electrolytes (for instance, 0.30 mA/cm^2 for 1 M $LiClO_4$ PC) were also within the same order of magnitude (typically < 1 mA/cm^2) as values noted in earlier works by EIS (**Table S1**). Significantly, when averaging across all cycles 1–50, a clear and positive correlation is observed between $j^p_{0,EIS}$ and CE across electrolytes (**Fig. 3c**). This trend also held true after a single cycle, when the magnitudes of $j^p_{0,EIS}$ were more similar across electrolytes, and continued to hold regardless of being averaged over 5, 10 and 20 galvanostatic

cycles, showing its generality regardless of the evolving $j^{p}_{0,EIS}$ values in Type 2 electrolytes (**Fig. S5**, ESI). Altogether, these results show clearly that interphases that allow fast Li^{+} exchange are associated with high CE, and that high-CE electrolytes uniquely exhibit dynamic behaviors in their $j^{p}_{0,EIS}$ values with cycling.

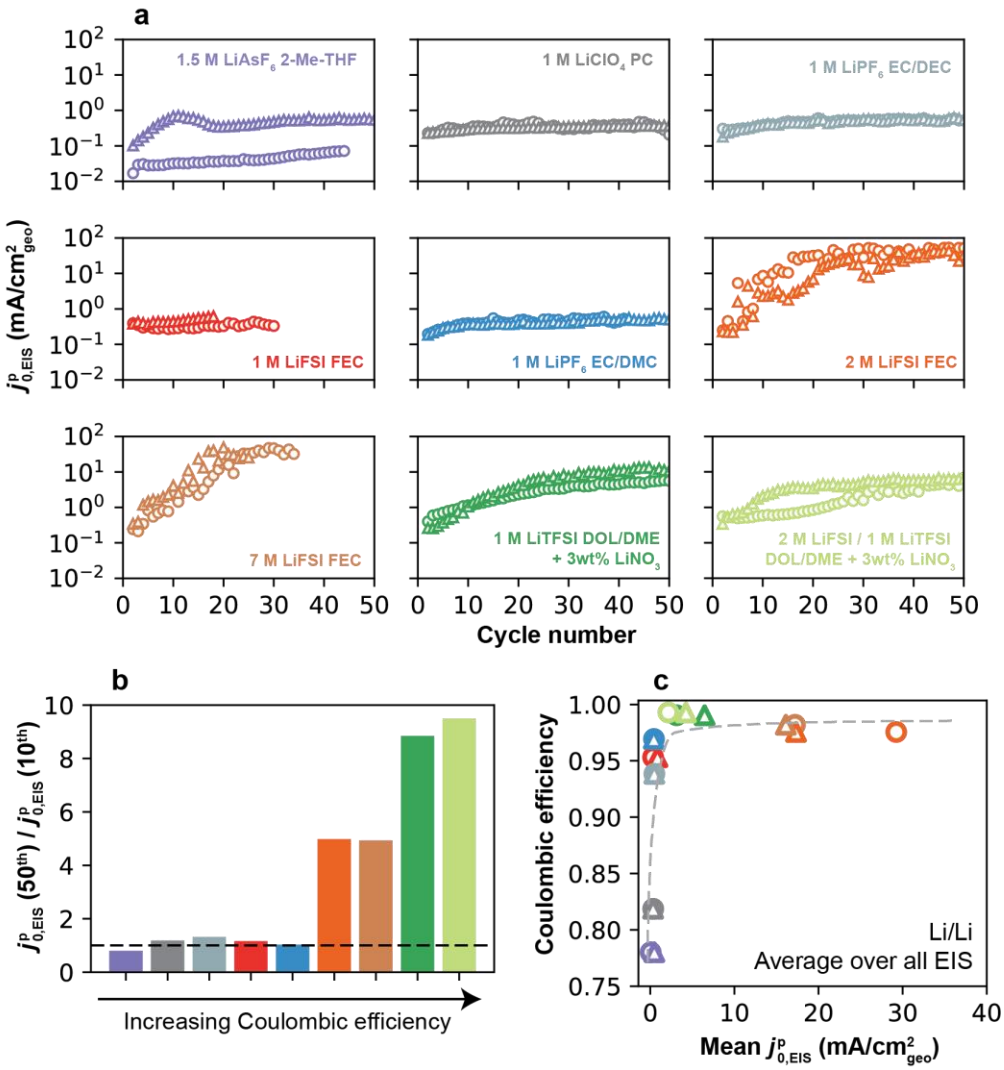

Fig. 3 Cycle-dependent Li^{+} exchange on Li anodes. (a) $j^{p}_{0,EIS}$ fitted from EIS spectra as a function of galvanostatic cycle number (1 mAh/cm² plating/stripping at 0.5 mA/cm²) in different electrolytes. Data were collected up to 50 cycles, or until apparent cell short-circuit (*i.e.*, 1 M LiFSI and 7 M LiFSI in FEC). (b) Relative increase in $j^{p}_{0,EIS}$ at the 50th (or last available) galvanostatic cycle compared to the 10th cycle. (c) Relationship between CE and $j^{p}_{0,EIS}$, where $j^{p}_{0,EIS}$ is averaged over all cycles in (a). Color legend of electrolytes in (b-c) as in (a).

Changes in $j^{p}_{0,EIS}$ over cycling can have two origins: (1) An increase in the intrinsic rate of Li^+ exchange of the SEI, such as from evolution in chemistry or changes in its thickness; (2) An increase in the electrochemically-active area for Li^+/Li^0 redox due to surface roughening. Both may occur in practice. While (1) is challenging to probe, (2) is undoubtedly a significant factor given the nonuniform nature of Li deposition. As observed by Lee *et al.*, low-CE electrolytes display a several-fold higher electrolyte-contact surface area compared to high-CE electrolytes after just a single cycle,[34] leading to higher porosity as well as formation of inactive Li^0 and SEI Li^+.[5] Curiously, the absence of any decreasing $j^{p}_{0,EIS}$ values in **Fig. 3a** suggests that the accumulation of these inactive materials does not suppress total Li^+ exchange rates, even in low-CE electrolytes. Additionally, a qualitative comparison between scanning electron microscopy (SEM) images of plated Li electrodes after 5 cycles in 1 M $LiPF_6$ EC/DMC and 1 M LiTFSI DOL/DME + 3wt% $LiNO_3$ confirms that these electrolytes are, as expected, porous after cycling, and that the lower-CE electrolyte shows higher surface area and more irregular deposits (**Fig. S6**, ESI).[35] Thus, the higher degree of porosity and surface area in the low-CE electrolytes do not translate into an increase in the rate of Li^+ exchange upon cycling in these electrolytes. This observation stands in contrast to high-CE electrolyte which, despite developing less SEI over a comparable number of cycles, displays significant increases in total Li^+ exchange rates. In other words, unlike in low-CE electrolytes, the additional surface created in high-CE electrolytes is active, as it allows Li^+ exchange between the electrolyte and the underlying Li metal, even if it forms to a comparatively lesser extent.

We more-carefully explored whether Li^+ exchange continued to increase unabatedly in high-CE electrolytes. Interestingly, $j^{p}_{0,EIS}$ for the DOL/DME-based electrolytes (exhibiting Type 2 behavior) further increased for approximately ten additional cycles, but did eventually stabilize around 60 cycles, *e.g.*, 8.3 mA/cm^2 for 2 M LiFSI 1 M LiTFSI DOL/DME + 3wt% $LiNO_3$ and 5.7 mA/cm^2 for 1 M LiTFSI DOL/DME + 3wt% $LiNO_3$ (**Fig. 4a**). This stable value was, however, much higher compared to low-CE electrolytes (0.39 mA/cm^2 for 1 M $LiClO_4$ PC, **Fig. 4a**). Although the underlying reasons for this behavior are not fully clear, a possible explanation is as follows (**Fig. 4b**). In low-CE electrolytes, the residual SEI has low Li^+ exchange values, thus provides little advantage for preferential nucleation of freshly-deposited Li in subsequent cycles. Because the SEI is not effectively re-utilized, subsequent Li plating requires re-establishment of the entirety of the SEI on each cycle, leading to lower CE. This regrowth process forms Li deposits

and SEI to a similar extent cycle-to-cycle for a fixed plating/stripping capacity. In contrast, in high-CE electrolytes, SEI residue from previous cycles may remain active for Li plating, and can be built-upon; hence, each cycle is history-dependent. These observations are consistent with cryo-EM evidence that demonstrate substantial necking and loss of active deposits upon stripping in low-CE electrolytes, whereas high-CE electrolytes show "reusable" SEI scaffolds that can be refilled on cycling.[36] We suggest that the eventual stabilization of Li^+ exchange in the high-CE electrolytes reflects a point at which the growth of new SEI scaffolds has completed, possibly due to their percolation throughout the electrode, although this point remains speculative at present. Overall, these findings indicate that "passivation", a commonly used term to describe the function of an SEI,[6, 32, 37, 38] has substantially different meaning depending on the system: while all SEIs at least minimally passivate Li against chemical reactivity with the electrolyte, some SEIs are inhibiting with respect to Li^+ exchange specifically, whereas others permit it.

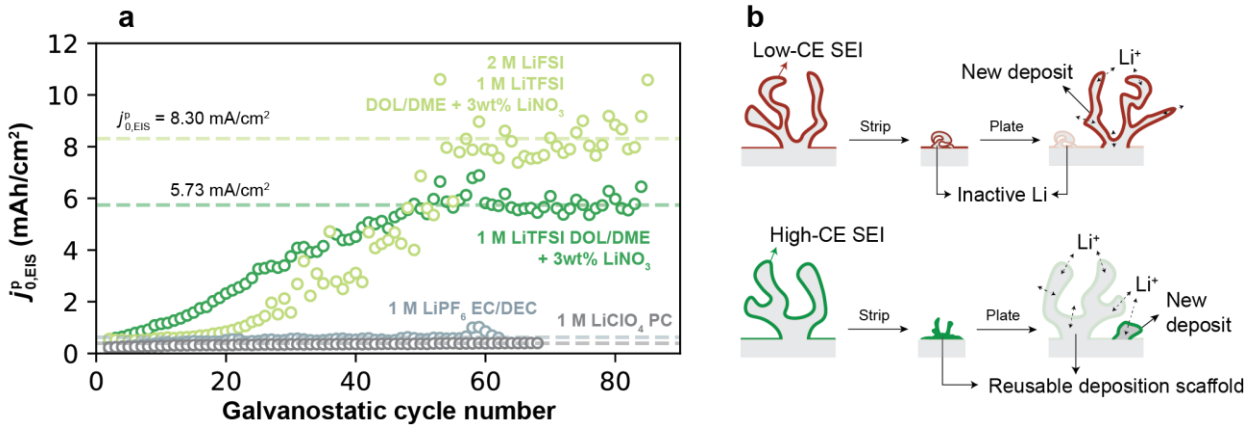

Fig. 4 Li^+ exchange over extended galvanostatic cycling. (a) $j^p_{0,EIS}$ as a function of cycle number of select low- and high-CE electrolytes, demonstrating eventual stabilization of Li^+ for the latter. (b) Illustration of a possible mechanism consistent with the observed dynamically-increasing Li^+ exchange values in high-CE electrolytes *vs.* stability of these values in low-CE electrolytes. Dark outlines on deposits denote SEI formation.

Determining Li^+ exchange by cyclic voltammetry

Li^+ exchange can also be determined from CV measurements during a plating/stripping step by evaluating the current-voltage slope around the Li^0/Li^+ equilibrium potential.[9] For the voltammetry analysis presented herein, coin cells were used to best capture conditions in a typical Li battery

with limited electrolyte volume (100 µL) and also to provide direct correspondence with the conditions used for EIS. In the adopted protocol (**Fig. 5a**), 11 continuous CV cycles were conducted in Cu/Li coin cells at 1 mV/s between -0.2 V and 1 V, with full stripping of Cu occurring on the end of each sweep. A single CV scan provides one data point for pseudo-Li^+ exchange current, which we here term $j^p_{0,CV}$ (**ESI Note 2**). To further compare values on a freshly deposited Li reservoir, 1 mAh/cm^2 of Li was galvanostatically plated at 0.5 mA/cm^2, followed by another set of 11 CV cycles from -0.2 V to 0.2 V. Finally, a full galvanostatic stripping step was conducted to 1 V to yield back a formed Cu current collector, followed by a final set of 11 CVs.

The current-voltage curves obtained on pristine Cu (**Fig. 5b**) in an exemplar 1 M $LiPF_6$ EC/DEC electrolyte show a typical behavior of metal deposition onto an inert substrate. On the forward scan, in which Li is first plated on Cu, an overpotential of ~100 mV is required to initiate Li plating on all cycles. On the reverse scan, Li continued to be plated on Cu until voltage exceeded the equilibrium potential (E^0, the voltage at which j = 0), after which Li was stripped from Cu. At low plating/stripping overpotential windows of this reverse scan (typically <20 mV, see **Fig. S7**, ESI), the magnitudes of the anodic and cathodic currents are small (< 0.2 mA/cm^2), and the current exhibits a linear response to overpotential. The slope of this response is proportional to $j^p_{0,CV}$ by $j = j^p_{0,CV}(RT/F)E_{\text{w,corrected}}$,[9] where $E_{\text{w,corrected}}$ is the measured potential corrected for ohmic losses and E^0 (Experimental methods, **ESI Note 2**). Fitting $j^p_{0,CV}$ at the linear limit avoids reliance on more complex kinetic models such as Tafel extrapolation, Butler-Volmer or Marcus-Hush formalisms that may be unphysical for interphase-dominated processes.[9]

Li^+ exchange for the pristine, Li-plated and fully-stripped Cu current collectors determined by this method are shown in **Fig. 5c**. In 1 M $LiPF_6$ EC/DEC, $j^p_{0,CV}$ is low for the pristine Cu electrode (0.02 mA/cm^2), but increases substantially and stabilizes to an average of 0.26 mA/cm^2 after Li is plated on the electrode. After Li is stripped away, $j^p_{0,CV}$ remains more similar to that of the Li-plated electrode than the pristine Cu electrode, *i.e.* is initially 0.40 mA/cm^2 in the 1st CV cycle before stabilizing around 0.19 mA/cm^2 in the 11th cycle. Altogether, these results confirm that Li plating behaviors are strongly dependent on surface conditioning and its history. Thus, in the following, we first examine the cross-electrolyte results on plated Li (middle column of **Fig. 5b**) for direct comparison with the EIS data, and later return to compare the differences between uncycled and cycled Cu.

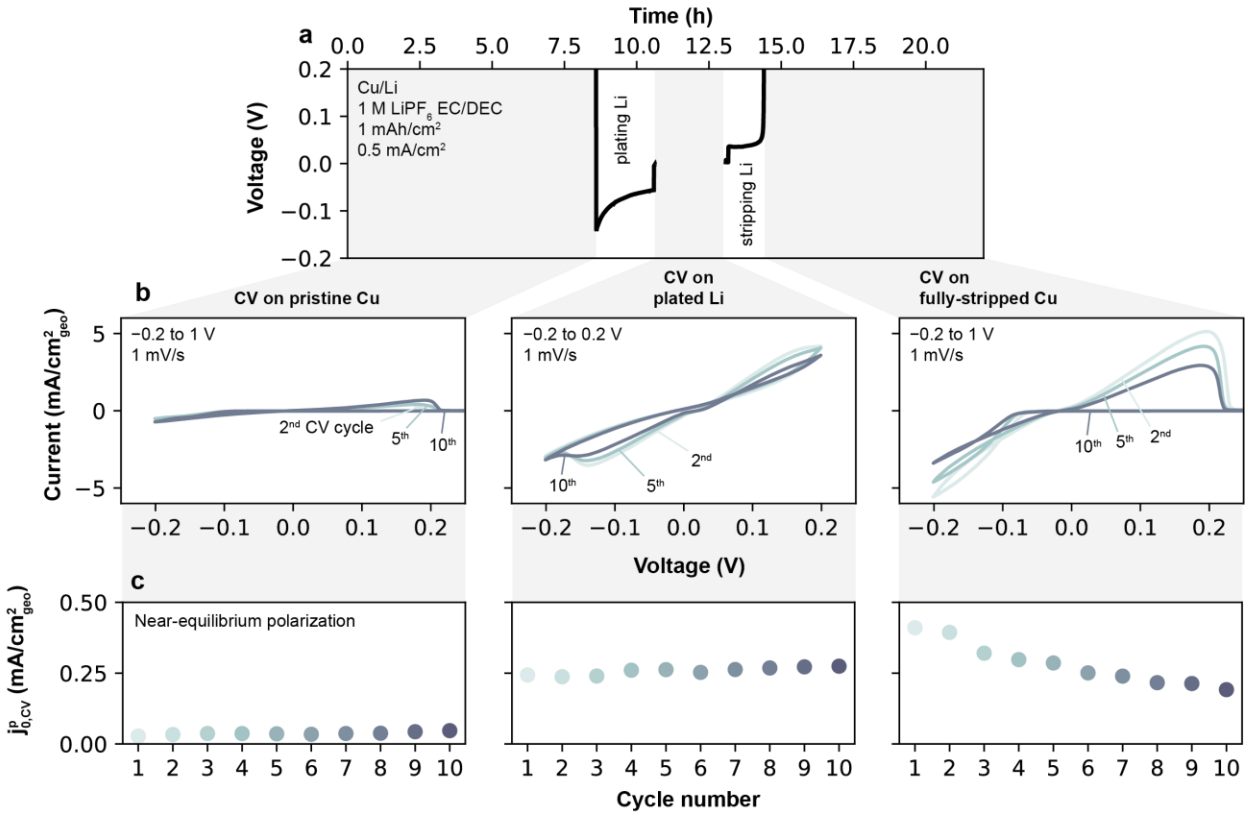

Fig. 5 Substrate-dependent cyclic voltammetry and extracted $j_{0,CV}^{p}$ of Li plating and stripping. (a) Procedure for obtaining $j_{0,CV}^{p}$ as a function of electrode condition (on Cu or plated Li), shown for an exemplar electrolyte, 1 M $LiPF_6$ EC/DEC. The gray regions denote periods of continuous CV scans. (b) Representative CV sweeps, from which $j_{0,CV}^{p}$ was obtained on each reverse scan. Following such CV scans on initially-pristine Cu, a Li reservoir of 1 mAh/cm^2 was plated galvanostatically as shown in (a), and CV cycling continued (second gray region and middle column). After 11 such CV cycles, Li was fully stripped, and an additional set of 11 CV cycles was conducted on the remaining formed Cu substrate. (c) $j_{0,CV}^{p}$ obtained from fitting CV data to the linear current-potential relationship near equilibrium as a function of CV cycle number.

Comparable voltammetry analysis on plated Li was performed in all other electrolytes. **Fig. 6a** shows Tafel plots for the three electrolytes highlighted in **Fig. 2**, where a steeper j-$E_{w,corrected}$ relationship near equilibrium indicates higher $j^p_{0,CV}$. The evolution of $j^p_{0,CV}$ as a function of CV scan number across all electrolytes is shown in **Fig. 6b**. First-scan values of $j^p_{0,CV}$ ranged from very low (0.01 mA/cm^2 for 1.5 M $LiAsF_6$ 2-Me-THF) to 1.21 mA/cm^2 in 2 M LiFSI FEC. In most electrolytes, $j^p_{0,CV}$ remained constant as a function of CV scan number. The high-CE DOL/DME-based electrolytes were notable exceptions, in which $j^p_{0,CV}$ increased monotonically with each CV scan, consistent with Type 2 behavior found from EIS. Critically, $j^p_{0,CV}$ and $j^p_{0,EIS}$ showed good agreement when values from both techniques are compared at similar accumulated Li cycling capacities (**Fig. 6c**), typically 1-9 mAh/cm^2 depending on the electrolyte (**ESI Note 3**). This agreement emphasizes that the obtained values of Li^+ exchange hold physical meaning, as they emerge to govern Li plating/stripping consistently regardless of measurement technique. Indeed, the same positive $j^p_{0,CV}$-CE correlation was observed on plated Li from CV measurements (**Fig. 6d**). We also observe that, for all electrolytes, the j-$E_{w,corrected}$ relationship shows typical Tafel behavior at high overpotentials, *i.e.*, linear $E_{w,corrected}$-log j behavior as seen in **Fig. 6a**. This behavior could be fitted well by Butler-Volmer[9] and Marcus-Hush-Chidsey[39] models at potentials below 100 mV (**Fig. S8**, ESI), even though such models do not consider an SEI. However, it is unclear at present whether this agreement carries any physical meaning.

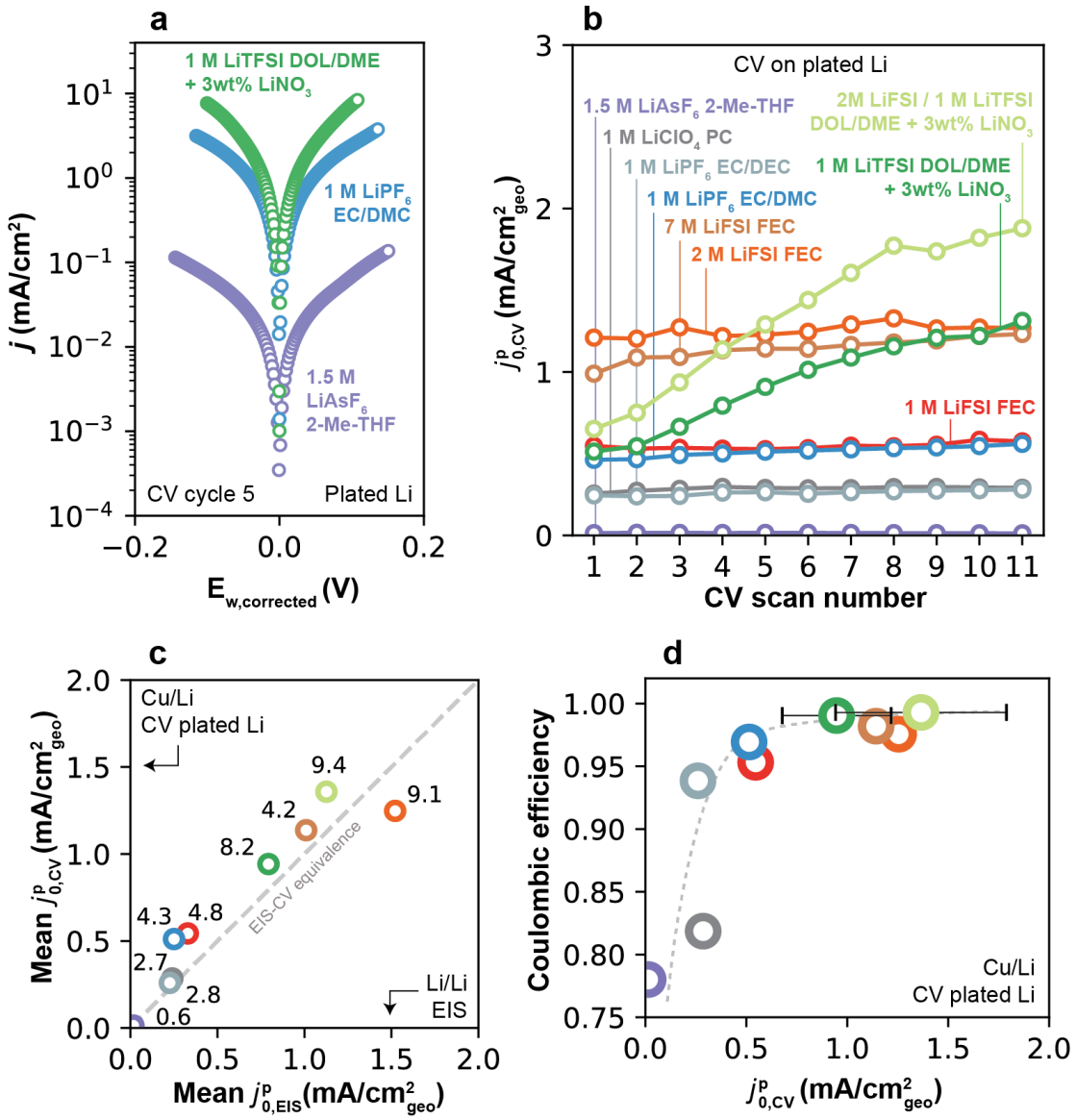

Fig. 6 Electrolyte-dependent Li^+ exchange captured by voltammetry on plated Li. (a) Tafel plot of select electrolytes measured by CV at 1 mV/s on 1 mAh/cm^2 of plated Li. (b) $j^p_{0,CV}$ as a function of CV scan number on plated Li for all electrolytes. (c) Comparison between mean $j^p_{0,CV}$ and mean $j^p_{0,EIS}$. $j^p_{0,CV}$ was averaged over 11 measurements on plated Li and $j^p_{0,EIS}$ was sampled at a cycle in which a comparable amount of Li (shown as marker labels in mAh/cm^2) had been cycled between CV and EIS. (d) CE-$j^p_{0,CV}$ relationship, with $j^p_{0,CV}$ calculated as the average over 11 cycles (same as (c)). Error bars represent standard deviation over all sequential CVs. Colors correspond to those in (b).

Inplications of the Cu formation cycle on j_0^p

We now return to compare j_0^p on the Cu substrate before and after significant amounts of Li have been cycled (**Fig. 5c**). **Fig. 7a** shows $j_{0,CV}^p$ over the first 11 CV scans on pristine Cu for all electrolytes. Given that unformed Cu surfaces typically exhibit low current densities, the total amount of charge plated/stripped was small (*e.g.*, ~0.03-0.3 mAh/cm^2 per cycle). In general, $j_{0,CV}^p$ values exhibited some scatter depending on the electrolyte but were typically low (<1 mA/cm^2). After the 1 mAh/cm^2 galvanostatic cycle (**Fig. 7b**), an evident upgrade in Li^+ exchange was observed in certain, but not all, electrolytes. This is further depicted in **Fig. 7c-d**, which summarize $j_{0,CV}^p$ on cycle 11 on the pre- and post-conditioned Cu, but now organized by CE. First, we observe that no correlation was found on Cu prior to the 1 mAh/cm^2 plating step (**Fig. 7c**), which is contrasted with post-plated Cu, where a strong monotonic trend was observed linking $j_{0,CV}^p$ and CE. This finding shows that, similar to the trends on Li, higher-CE electrolytes are also more effective at modifying the Cu interface, an effect that persists even after full galvanostatic stripping of the underlying Li. In contrast, low-CE electrolytes display minimal difference in Li^+ exchange between pre-plated and stripped Cu, indicating that SEI formation on Cu is ineffective in these electrolytes even after a 1 mAh/cm^2 cycle. The quantitative CE-$j_{0,CV}^p$ monotonic relationship specific to post-stripped Cu is fully summarized in **Fig. 8**. Even when subjected to repeated 1 mAh/cm^2 plating/stripping cycles, Type 1 electrolytes could not reach Li^+ exchange rates comparable to those achieved after just a single cycle in Type 2 electrolytes (**Fig. S9**, ESI).

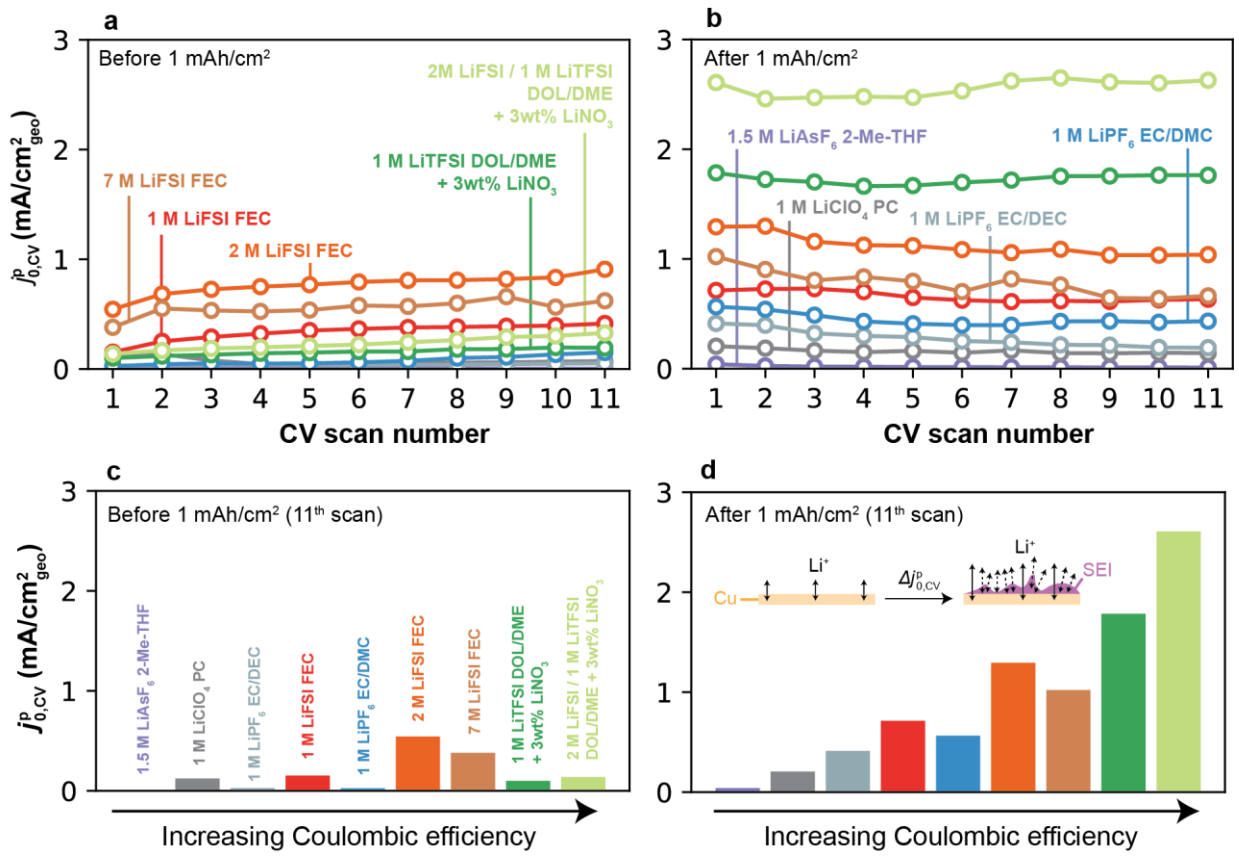

Fig. 7 Effect of the Cu formation cycle on Li^+ exchange and CE. (a) $j^p_{0,CV}$ as a function of CV scan number on pristine Cu. (b) $j^p_{0,CV}$ as a function of CV scan number on cycled Cu. (c) $j^p_{0,CV}$ measured on the 11th CV scan on Cu prior to a 1 mAh/cm^2 galvanostatic formation cycle. (d) $j^p_{0,CV}$ measured on the 11th CV scan following the 1 mAh/cm^2 galvanostatic formation cycle. Inset represents an illustration of a possible mechanism for the observed upgrade in Li^+ exchange after Cu formation. The protocol in **Fig. 5** was used to collect all data. Color legend in (d) as in (a-c).

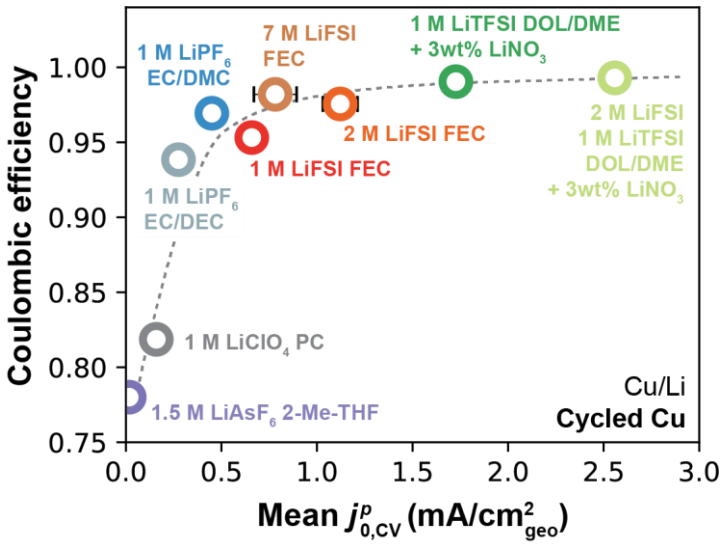

Fig. 8 Li CE *vs.* $j^{p}_{0,CV}$ measured on cycled Cu after the 1 mAh/cm^2 formation cycle, averaged over 11 CV cycles. Error bars denote standard deviation over all 11 CV cycles.

The previous correlations relate $j^{p}_{0,CV}$ measured on a per-cycle basis to an averaged, representative CE value in each electrolyte. To further explore the connection between Li^+ exchange and CE as the SEI is formed on Cu, we exploited the fact that CV measurements enable the calculation of CE and Li^+ exchange concomitantly on each scan. This $j^{p}_{0,CV}$-CE relationship is shown in **Fig. 9a** for 1 M $LiPF_6$ EC/DEC (Type 1 electrolyte) and **Fig. 9b** for 2 M LiFSI 1 M LiTFSI DOL/DME + 3wt% $LiNO_3$ (Type 2 electrolyte); these data were obtained from the same CV scans underlying **Fig. 7a-b**. Focusing first on the Type 1 electrolyte (**Fig. 9a**), a monotonic increase in per-cycle CE was observed with increasing $j^{p}_{0,CV}$ from cycles 1-10. Following a 1 mAh/cm^2 galvanostatic cycle, $j^{p}_{0,CV}$ exhibited a step-change increase to higher values, with accompanying improvements in CE. A similar behavior was observed in the Type 2 electrolyte (**Fig. 9b**), though expectedly with much higher CE and $j^{p}_{0,CV}$. These results agree with our previous findings on the relationship between these two parameters, but it also highlights a subtle new insight: CE is also coupled to Li^+ exchange on a per-cycle basis. In this context, the lower first-cycle CE typically found in anode-free batteries[26, 40] can be physically explained by an inability of the uncycled Cu to accommodate fast Li^+ exchange. This $j^{p}_{0,CV}$-CE coupling is further explored in **ESI Note 4**, where experimental evidence of a continuous relationship between $j^{p}_{0,CV}$ and CE during SEI formation on Cu is presented.

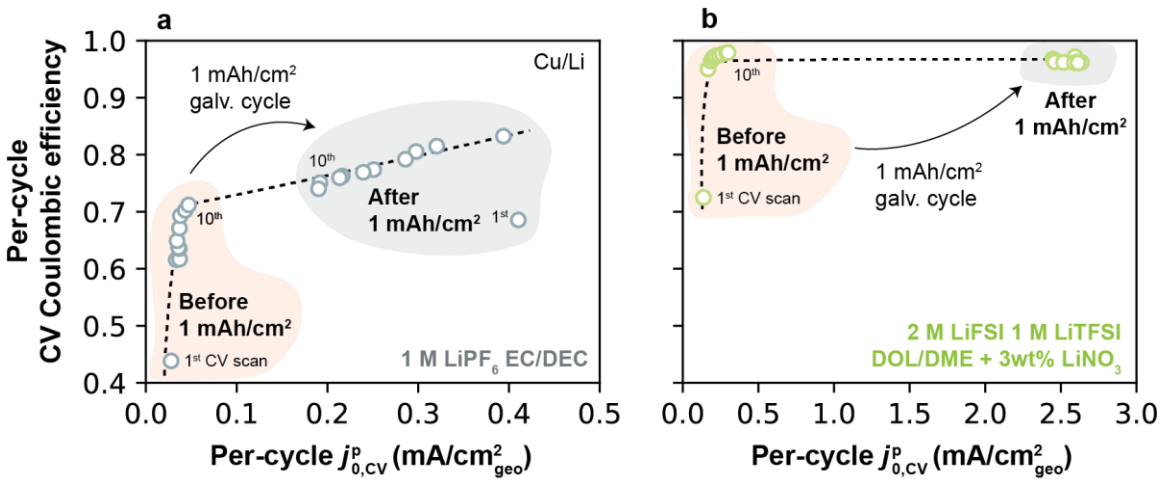

Fig. 9 Per-cycle CE and $j^{p}_{0,CV}$ obtained by CV on Cu, before and after a full 1 mAh/cm^2 galvanostatic cycle in (a) 1 M $LiPF_6$ EC/DEC; and (b) 2 M LiFSI 1 M LiTFSI DOL/DME + 3wt% $LiNO_3$.

Implications of j_0^p on Li rate capability

Finally, we examined the implications of Li^+ exchange on the rate capability (here defined as CE *vs.* cycling current density) attainable in different electrolytes. As extensively discussed, Li^+ exchange quantifies the facility by which an SEI exchanges Li^+ from the electrolyte to the electrode. Thus, in addition to its relationship to CE, we hypothesized that the rate of SEI Li^+ exchange defines the maximum cycling current density j at which Li can be cycled without substantial decline in CE. For this analysis, we focused on the Li^+ exchange obtained by EIS ($j^{p}_{0,\mathrm{EIS}}$) which was measured between galvanostatic cycles, a protocol that is most relevant to how CE is typically measured. The Type 1 and Type 2 electrolytes tested herein exhibit two distinct regimes: Type 1 electrolytes show $j^{p}_{0,\mathrm{EIS}}$ < 1 mA/cm^2, a value that is in the range of typical cycling currents used in Li anode studies (0.1–2 mA/cm^2). Type 2 electrolytes, however, can sustain $j^{p}_{0,\mathrm{EIS}}$ exceeding 10 mA/cm^2, a value well-beyond typical cycling currents.

In this context, **Fig. 10** shows CE as a function of current density (see **Fig. S1**, ESI, for protocol) for select electrolytes spanning Type 1 and Type 2 behaviors. Interestingly, the CE in Type 1 carbonate electrolytes (1 M $LiPF_6$ EC/DEC and 1 M $LiClO_4$ PC) is less stable with increasing j, showing general decline at high j when compared to their respective CE measured at j < 0.5 mA/cm^2. This behavior is most evident in 1 M $LiClO_4$ PC, in which CE decreases from

87.1% to 76.9% between 0.2 mA/cm^2 and 2 mA/cm^2. On the other hand, the Type 2 electrolytes (2 M LiFSI FEC and DOL/DME-based electrolytes) have CE values invariant with cycling current j. These observations can be interpreted in light of the applied current with respect to the SEI Li^+ exchange capability. In 1 M $LiClO_4$ PC and 1 M $LiPF_6$ EC/DEC, $j^p_{0,\mathrm{EIS}}$ never exceeds 0.25 mA/cm^2 and 0.55 mA/cm^2, respectively; these electrolytes displayed substantial loss of CE when the applied current density exceeds these values. On the other hand, the rate-independence observed by the Type 2 electrolytes may be attributed to the extreme Li^+ exchange rates that SEI in those systems can tolerate, which can easily exceed 5 mA/cm^2 (**Figs. 3-4**). Interestingly, Type 2 electrolytes exhibit variable Li^+ exchange under stress conditions (such as continued cycling), a factor that may enhance their ability to cycle well at high rate compared to Type 1 electrolytes. Because growth of SEI surface area increases total Li^+ exchange, it is possible that non-uniform Li deposition is not necessarily detrimental and may even be beneficial for high cycling currents in these electrolytes, as long as such deposits remain electronically-percolated. We further note that, when j^p_0 is very high, other rate-limiting factors may become relevant before the SEI becomes the major bottleneck. For instance, j^p_0 can reach values >5 mA/cm^2 in Type 2 electrolytes; under these conditions, mass transport at the bulk electrolyte may become limiting prior to SEI Li^+ exchange.[41] Further studies on this interplay, and transition between limiting regimes,[4] are expected to be fruitful.

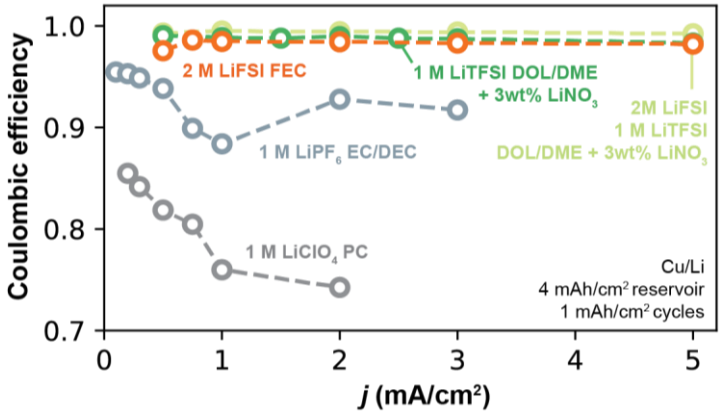

Fig. 10 CE as a function of rate for select Type 1 (low and stable j^p_0) and Type 2 (high and increasing j^p_0) electrolytes.

Conclusion

Total Li^+ exchange through natively-formed Li SEIs was quantified in a selection of low- and high-CE electrolytes using two electrochemical techniques, EIS and CV. These methods offer unique but complementary approaches for quantification of Li^+ exchange rates, and produced self-consistent values in each given electrolyte, providing confidence in the physicality of the obtained values. Low-CE electrolytes typically displayed stable and modest rates of Li^+ exchange (<1 mA/cm^2), *i.e.*, on the order of typical battery cycling currents. On the other hand, high-CE electrolytes exhibited higher total Li^+ exchange rates that further increased over cycling. A tight positive correlation was found between CE and Li^+ exchange even when accounting for these dynamic effects, thus demonstrating unambiguously that electrolytes that enable fast Li^+ exchange correlate with high CE. Our results also revealed that Li^+ exchange is more sluggish on uncycled *vs.* cycled Cu, with correspondingly lower CE on pristine Cu, providing insights into underlying processes occurring during the first plating step. Looking forward, we anticipate that these findings may support new frameworks for electrolyte design to maximize SEI phases that promote facile Li^+ exchange, once such phases can be better identified with chemical specificity, and for the advancement of formation protocols and surface engineering of Cu which, as our work shows, can have profound effects on both Li^+ exchange and reversibility.

Experimental methods

Materials preparation

Dimethyl carbonate (DMC, Acros Organics), 1,3-dioxolane (DOL), 2-methyl-tetrahydrofuran (2-Me-THF, MilliporeSigma), 1,2-dimethoxyethane (DME), and fluoroethylene carbonate (FEC, Tokyo Chemical Industry) solvents were dried under molecular sieves (4Å, MilliporeSigma) for at least 36 h before use. Lithium bis(fluorosulfonyl)imide (LiFSI, Arkema), lithium bis(trifluoromethanesulfonyl)imide (LiTFSI, Tokyo Chemical Industry) and lithium nitrate ($LiNO_3$, Tokyo Chemical Industries) salts were dried at 110 °C in a vacuum glass oven (Buchi) before use. Lithium hexafluoroarsenate(V) ($LiAsF_6$, Strem) was used as-received. Battery-grade 1 M $LiPF_6$ ethylene carbonate (EC)/diethyl carbonate (DEC) and 1 M $LiPF_6$ EC/DMC (1:1 vol%, MilliporeSigma) were used as-received. All other electrolytes were prepared in an Ar-filled glovebox (MBraun, <0.1 ppm O_2, <0.1 ppm H_2O). Li metal foil (ø0.75 mm, Alfa Aesar) was rolled and cut into ø15 mm diameter disks immediately before use. Cu foil (MTI) was punched to ø15 mm diameter, acid-washed with 1 M H_2SO_4 for 1 h, cleaned with deionized (DI) water (MilliQ, >18.2 MΩ/cm), rinsed with acetone and immediately dried under vacuum at room temperature for at least 8 h under antechamber vacuum. Coin cell components (CR2032, MTI) were cleaned with ethanol followed by DI water and dried before use. Glass fiber separators (Whatman QM-A) were punched to ø16 mm diameter and dried in a vacuum glass oven at 130 °C before use. Microporous polymeric separators (Celgard 2325 and 3501) were punched to ø20 mm diameter and dried under antechamber vacuum for at least 8 h before use.

Cell assembly

CR2032 coin cells were assembled inside an Ar-filled glovebox (Mbraun, <0.1 ppm H_2O, <0.1 ppm O_2). Li strips were rolled into thin films, punched to ø15 mm diameter, then pressed into stainless steel current collectors and used as counter/reference electrode for all measurements. For measurements in Li/Li cells, another identical piece of Li film pressed into a stainless steel current collector was used as the working electrode. For measurements in Cu/Li cells, Cu was used as the working electrode with a stainless steel current collector. For general electrochemical measurements, one Whatman glass fiber, soaked in 100 µL of the desired electrolyte, was used per cell. For SEM characterization, two separators (either Celgard 2325 or 3501) were used per cell,

along with a total of 50 µL of the desired electrolyte. The assembled CR2032 was closed with a wave spring, crimped and taken outside the glovebox for testing.

Coulombic efficiency

Coulombic efficiency (CE) measurements were conducted as described by Adams *et al*.[26] in Cu/Li cells. All measurements include a single formation cycle, plating 4 mAh/cm^2 Li on Cu and then stripping until all reversible Li is depleted to 1 V at 0.5 mA/cm^2. A Li reservoir of 4 mAh/cm^2 is then plated onto Cu, and 1 mAh/cm^2 from the reservoir is cycled 10 times, after which the reservoir is completely stripped to 1 V. Between each half-cycle, the cell rests at open-circuit voltage (OCV) for 1 min. CE is determined as the ratio of the total amount of Li stripped to the total amount plated, excluding the formation cycle. For all measurements, the formation cycle was performed at 0.5 mA/cm^2 but current density for reservoir cycling was performed at the indicated current density. **Fig. S1**, ESI, demonstrates the CE measurement protocol. All CE measurements were conducted on a battery cycler (BTS, MTI).

Electrochemical impedance spectroscopy

Electrochemical impedance spectroscopy (EIS) measurements were conducted in Li/Li cells that were taken outside of the glovebox immediately after cell assembly. EIS spectra were collected on Biologic MPG or VSP-3 potentiostats with a sine-wave excitation amplitude of 5 mV around OCV, with a typical frequency range of 10 mHz to 20 kHz, with 10 points collected per decade. Before the initial EIS measurement, the cell rested at OCV for 5 h.

After the spectra were collected, the single semi-circle (typically corresponding to frequencies >20 Hz) was fit to an equivalent resistor-capacitance-Warburg circuit, where the RC impedance represents the Li^0/Li^+ redox charge-transfer resistance and the Warburg impedance represents diffusional transport across the interphase.[33] The circuit was fit to data using a custom Python script that employs a least-square method. The total resistance to interface exchange (R_{SEI}) was taken as the sum of the Warburg coefficient (W_1) and the charge-transfer resistance R_{ct} to capture all SEI-relevant processes including charge transfer (kinetics) and transport, which are physically coupled in a thin but finite SEI. The equivalent EIS exchange current ($j^{p}_{0,EIS}$) is then inversely proportional to the total SEI resistance (R_{SEI})[9] such that

$$j^{p}_{0,\mathrm{EIS}} = \frac{kT}{neR_{SEI}},$$

where k is the Boltzmann constant, T is the temperature, n is the number of electrons transferred per reaction (n = 1 for Li^+/Li redox) and e is the electron charge. See **ESI Note 1** for more information on the fitting process.

Cyclic voltammetry

Cyclic voltammetry (CV) data were acquired in two-electrode coin cells using Biologic MPG or VSP-3 potentiostats, with a typical scan rate of 1 mV/s unless otherwise mentioned. For experiments where Cu was the working electrode (*i.e.*, pristine or fully-stripped Cu), the measurement started at OCV (typically ~3 V for pristine Cu and ~0 V for fully-stripped Cu) and voltage was scanned from OCV to -0.2 V, and then from -0.2 V to 1 V, cycling within the voltage window for the desired number of cycles. For experiments where Li was the working electrode (*i.e.*, plated Li), the measurement starts at OCV (~0 V) and voltage was scanned from OCV to -0.2 V, and then between -0.2 V to 0.2 V, for the desired number of cycles. All CV cycles were conducted continuously. In order to obtain $j^{p}_{0,CV}$, the CV data was processed such that, first, the cell voltage was iR-compensated and corrected such that the potential at zero current was set to zero (*i.e.*, $E_{w,corrected}(j = 0) = 0$ V). Then, data in the low-overpotential regime, where the current response is linear with overpotential, was used to obtain a representative exchange current $j^{p}_{0,CV}$ such that $j = j^{p}_{0,CV}\ (F/RT)\ E_{w,corrected}$, thus avoiding the use of more complex kinetic models or Tafel interpolation at high overpotentials that may yield unphysical results for interphase-dominated processes.[9] More information on the CV analysis is presented in **ESI Note 2**.

Acknowledgements

The authors acknowledge a collaborative grant from the Sagol Weizmann-MIT Bridge Program. This work made use of the MRSEC Shared Experimental Facilities at MIT, supported by the National Science Foundation under award number DMR-1419807. This work also made use of the Department of Chemistry Instrumentation Facility (DCIF) at MIT.

Author contributions

G.M.H. and B.M.G conceptualized the study and analyzed the data; G.M.H. performed experiments, acquired and processed the data; K.H.K. acquired SEM images of cycled electrodes. B.M.G. supervised data acquisition and processing; G.H.M and B.M.G. wrote, edited and reviewed all drafts of the manuscript.

Conflicts of interest

None to report.

References

1. H. Wang, Z. Yu, X. Kong, S. C. Kim, D. T. Boyle, J. Qin, Z. Bao and Y. Cui, *Joule*, 2022, **6**, 588-616.
2. J. Zheng, M. S. Kim, Z. Tu, S. Choudhury, T. Tang and L. A. Archer, *Chem. Soc. Rev.*, 2020, **49**, 2701-2750.
3. P. Albertus, S. Babinec, S. Litzelman and A. Newman, *Nat. Energy*, 2017, **3**, 16-21.
4. G. M. Hobold, J. Lopez, R. Guo, N. Minafra, A. Banerjee, Y. Shirley Meng, Y. Shao-Horn and B. M. Gallant, *Nat. Energy*, 2021, **6**, 951-960.
5. C. Fang, J. Li, M. Zhang, Y. Zhang, F. Yang, J. Z. Lee, M. H. Lee, J. Alvarado, M. A. Schroeder, Y. Yang, B. Lu, N. Williams, M. Ceja, L. Yang, M. Cai, J. Gu, K. Xu, X. Wang and Y. S. Meng, *Nature*, 2019, **572**, 511-515.
6. A. B. Gunnarsdottir, C. V. Amanchukwu, S. Menkin and C. P. Grey, *J. Am. Chem. Soc*, 2020, **142**, 20814-20827.
7. Y.-C. Hsieh, M. Leißing, S. Nowak, B.-J. Hwang, M. Winter and G. Brunklaus, *Cell. Rep. Phys. Sci.*, 2020, **1**, 100139.
8. C. Fang, B. Lu, G. Pawar, M. Zhang, D. Cheng, S. Chen, M. Ceja, J.-M. Doux, H. Musrock, M. Cai, B. Liaw and Y. S. Meng, *Nat. Energy*, 2021, **6**, 987-994.
9. A. J. Bard and L. R. Faulkner, *Electrochemical methods : fundamentals and applications*, John Wiley & Sons, Hoboken, 2007.
10. D. T. Boyle, X. Kong, A. Pei, P. E. Rudnicki, F. Shi, W. Huang, Z. Bao, J. Qin and Y. Cui, *ACS Energy Lett.*, 2020, **5**, 701-709.
11. A. B. Gunnarsdóttir, S. Vema, S. Menkin, L. E. Marbella and C. P. Grey, *J. Mater. Chem. A*, 2020, **8**, 14975-14992.
12. J. N. Butler, D. R. Cogley and J. C. Synnott, *J. Phys. Chem.*, 2002, **73**, 4026-4027.
13. M. W. Verbrugge and B. J. Koch, *J. Electroanal. Chem.*, 1994, **367**, 123-129.
14. S. G. Meibuhr, *J. Electrochem. Soc.*, 1970, **117**, 56.
15. R. F. Scarr, *J. Electrochem. Soc.*, 1970, **117**, 295-&.
16. S. G. Meibuhr, *J. Electrochem. Soc.*, 1971, **118**, 1320-&.
17. R. Tao, X. Bi, S. Li, Y. Yao, F. Wu, Q. Wang, C. Zhang and J. Lu, *ACS. Appl. Mater. Interfaces*, 2017, **9**, 7003-7008.
18. K. S. Aojula, J. D. Genders, A. D. Holding and D. Pletcher, *Electrochim. Acta*, 1989, **34**, 1535-1539.
19. C. C. Su, M. He, J. Shi, R. Amine, J. Zhang and K. Amine, *Angew. Chem.*, 2020, **59**, 18229-18233.
20. X. Fan, L. Chen, O. Borodin, X. Ji, J. Chen, S. Hou, T. Deng, J. Zheng, C. Yang, S. C. Liou, K. Amine, K. Xu and C. Wang, *Nat. Nanotechnol.*, 2018, **13**, 715-722.
21. Q. Zhao, Z. Tu, S. Wei, K. Zhang, S. Choudhury, X. Liu and L. A. Archer, *Angew. Chem.*, 2018, **57**, 992-996.
22. X.-Q. Zhang, X. Chen, L.-P. Hou, B.-Q. Li, X.-B. Cheng, J.-Q. Huang and Q. Zhang, *ACS Energy Lett.*, 2019, **4**, 411-416.
23. F. Shi, A. Pei, D. T. Boyle, J. Xie, X. Yu, X. Zhang and Y. Cui, *Proc. Natl. Acad. Sci. U.S.A.*, 2018, **115**, 8529-8534.
24. Y. Liu, X. Xu, M. Sadd, O. O. Kapitanova, V. A. Krivchenko, J. Ban, J. Wang, X. Jiao, Z. Song, J. Song, S. Xiong and A. Matic, *Adv. Sci.*, 2021, **8**, 2003301.
25. F. Shi, A. Pei, A. Vailionis, J. Xie, B. Liu, J. Zhao, Y. Gong and Y. Cui, *Proc. Natl. Acad. Sci. U.S.A.*, 2017, **114**, 12138-12143.

26. B. D. Adams, J. Zheng, X. Ren, W. Xu and J. G. Zhang, *Adv. Energy Mater.*, 2017, **8**.
27. P. Bai, J. Li, F. R. Brushett and M. Z. Bazant, *Energy Environ. Sci.*, 2016, **9**, 3221-3229.
28. Y. Chen, Z. Yu, P. Rudnicki, H. Gong, Z. Huang, S. C. Kim, J. C. Lai, X. Kong, J. Qin, Y. Cui and Z. Bao, *J. Am. Chem. Soc.*, 2021, **143**, 18703-18713.
29. Z. Yu, H. Wang, X. Kong, W. Huang, Y. Tsao, D. G. Mackanic, K. Wang, X. Wang, W. Huang, S. Choudhury, Y. Zheng, C. V. Amanchukwu, S. T. Hung, Y. Ma, E. G. Lomeli, J. Qin, Y. Cui and Z. Bao, *Nat. Energy*, 2020, **5**, 526-533.
30. D. Aurbach and A. Zaban, *J. Electroanal. Chem.*, 1993, **348**, 155-179.
31. M. Odziemkowski and D. E. Irish, *J. Electrochem. Soc.*, 2019, **140**, 1546-1555.
32. D. T. Boyle, W. Huang, H. Wang, Y. Li, H. Chen, Z. Yu, W. Zhang, Z. Bao and Y. Cui, *Nat. Energy*, 2021, **6**, 487-494.
33. A. Zaban, E. Zinigrad and D. Aurbach, *J. Phys. Chem.*, 1996, **100**, 3089-3101.
34. J. Z. Lee, T. A. Wynn, M. A. Schroeder, J. Alvarado, X. Wang, K. Xu and Y. S. Meng, *ACS Energy Lett.*, 2019, **4**, 489-493.
35. J. Qian, W. A. Henderson, W. Xu, P. Bhattacharya, M. Engelhard, O. Borodin and J. G. Zhang, *Nat. Commun.*, 2015, **6**, 6362.
36. Y. Li, W. Huang, Y. Li, A. Pei, D. T. Boyle and Y. Cui, *Joule*, 2018, **2**, 2167-2177.
37. E. Peled and S. Menkin, *J. Electrochem. Soc.*, 2017, **164**, A1703-A1719.
38. S. K. Heiskanen, J. Kim and B. L. Lucht, *Joule*, 2019, **3**, 2322-2333.
39. Y. Zeng, R. Smith, P. Bai and M. Z. Bazant, *arXiv*, 2014, arXiv:1407.5370.
40. J. Xiao, Q. Li, Y. Bi, M. Cai, B. Dunn, T. Glossmann, J. Liu, T. Osaka, R. Sugiura, B. Wu, J. Yang, J.-G. Zhang and M. S. Whittingham, *Nat. Energy*, 2020, **5**, 561-568.
41. J. Zheng, M. S. Kim, Z. Tu, S. Choudhury, T. Tang and L. A. Archer, *Chem Soc Rev*, 2020, **49**, 2701-2750.